BİTLİS EREN ÜNİVERSİTESİ
FEN BİLİMLERİ DERGİSİ

ISSN: 2147-3129 / e-ISSN: 2147-3188

Article Type	: Research Article	**Year**	: 2025
Received	: November 13, 2024	**Volume**	: 14
Revised	: March 7, 2025	**Issue**	: 2
Accepted	: June 24, 2025	**Pages**	: 732-754
DOI	: 10.17798/bitlisfen.1584811		

EFFECTS OF INTERACTIONS BETWEEN INDIVIDUALS AND SPATIAL DYNAMICS ON THE SPREAD OF INFECTIOUS DISEASES USING VORONOI TESSELLATION AND THE ISING MODEL

Şeyma Firdevs HIZAL [1], **Hasan BULUT** [1, 2, *]

[1] *Fırat University, Department of Mathematics, Elazığ, Türkiye*

[2] *Azerbaijan University, Department of Mathematics and Informatics, Baku, Azerbaijan*

**** Corresponding Author:*** *hbulut@firat.edu.tr*

ABSTRACT

This study investigates the spatial distribution of individuals within a randomly distributed sample population and their interactions with an infectious disease. For this purpose, an Ising model enhanced with Voronoi tessellation is used to create a more realistic framework for modeling disease spread. The model simulates the process of spreading infectious disease by considering the interactions between individuals and their movement dynamics. The sample population in this study was created for simulation purposes only and is not based on actual demographic of epidemiological data. To assess the infectiousness in the model, the parameter J, defined as the transmission coefficient, is analyzed.

Keywords: Voronoi tessellation, Ising model, Monte Carlo simulations, Metropolis algorithm, Disease spread, Epidemiological modelling.

1 INTRODUCTION

Epidemics are infections that disrupt the normal functioning of biological organisms and pose serious threats to public health. They are characterized by the rapid spread of pathogens among human populations and can affect large populations in a short time, placing a heavy burden on health systems [1]. Epidemics are complex biological and scientific processes that profoundly affect individual health and social, economic and political structures. Infections

caused by pathogens such as viruses, bacteria or parasites through their interactions with host organisms can spread through direct contact, airborne transmission, water or vectors [2]. Indeed, recent pandemics such as COVID-19 have dramatically demonstrated the speed and global impact of the spread of such pathogens [3].

Historically, epidemics have led to significant social, economic and political transformations. For example, the Black Plague in Europe in the 14th century caused the death of a large portion of the population and reshaped the social order [4]. Similarly, the Spanish flu pandemic of 1918 killed millions of people worldwide and created significant disruptions in the global economy after the pandemic [5]. More recent pandemics, such as the HIV/AIDS pandemic and the COVID-19 pandemic, have put immense pressure on global health systems, leading to widespread crises in both individual and public health [6], [7].

Understanding the dynamics of epidemic disease spread plays a crucial role in combating these diseases. Mathematical epidemiology, a sub-discipline of epidemiology, was developed to model how infectious diseases spread in populations [8]. Mathematical models are employed to predict disease spread within a population, changes in the number of infected individuals, and the effects of various intervention strategies. In this context, the first mathematical models created by Daniel Bernoulli in the 18th century to analyze the spread of smallpox have become foundational to modern epidemiology [9]. Bernoulli's work marks a significant advancement in strategies aimed at reducing mortality rates and understanding the effects of diseases on populations. Later, the SIR (Susceptible-Infectious-Recovered) model, developed by Kermack and McKendrick in 1927, emerged as a fundamental aspect of modern epidemiology and has been extensively used to study the dynamics of infectious diseases such as measles, mumps, and influenza [10]. The SIR model possesses a straightforward yet powerful structure that categorizes individuals as “susceptible,” “infectious,” and “recovered.” However, the SIR model is a homogeneous framework that overlooks the effects of spatial interactions and fails to fully capture the complex interactions among individuals [11]. To address these shortcomings, more detailed models have been formulated for diseases that exhibit specific incubation periods, such as the SEIR (Susceptible-Exposed-Infectious-Recovered) model [12]. For example, the SEIR epidemic model has been utilized to explore the transmission dynamics of malaria by illustrating the dependence of mosquito populations on human populations and the impact of environmental factors on disease spread [13]. Similarly, the SEIR model has also been applied to investigate the transmission dynamics of dengue fever [14]. Although the SEIR model provides a more nuanced understanding of the

transmission dynamics of specific pathogens, its exclusion of spatial distribution and individual interactions remains a significant drawback.

Due to their rapid and analytical solutions, classical epidemic models (SI, SIS, SIR, SEIR, etc.) are often preferred as practical tools for predicting the dynamics of general outbreaks. One of their primary advantages is the ease with which they allow for the calculation of fundamental epidemiological parameters, such as the basic reproduction number (R_0). However, by assuming a homogeneous population and evaluating contact rates through a single parameter, these models face significant limitations in capturing the heterogeneous and irregular distribution of individuals observed in real-world conditions [15]. In particular, in scenarios where spatial heterogeneity and local interactions play a critical role, the forecasts provided by classical models can be lacking. Consequently, obtaining a more comprehensive understanding of how individual mobility and spatial interactions influence epidemic dynamics is crucial for modeling disease spread more realistically. This need has spurred the development of more complex and realistic models, while spatially oriented approaches have emerged as a growing area of research in epidemiological modeling in recent years [16]. In this context, the significance of various geometric methods designed to more accurately model spatial dynamics has steadily increased. Among these methods, Voronoi tessellation provides a way to represent individuals' spatial proximity and interaction domains more realistically by geometrically identifying the nearest regions surrounding each point in a set [17]. Through this approach, cells are generated around each seed point to include the nearest points, thereby clearly delineating the boundaries of potential interactions among individuals [18]. Consequently, Voronoi tessellation, widely employed in fields such as computational geometry, neuronal distribution, and urban planning [19], [20], enhances epidemiological analyses by offering a more realistic depiction of spatial patterns and local contact relationships, thus addressing gaps in existing models.

Meanwhile, the Ising model, introduced in the 1920s by German physicist Ernst Ising, was originally developed as a theoretical framework to explore the interactions among atoms or spins in crystal lattices [21], [22]. In this model, each atom or spin can exist in one of two possible states: up (plus 1) or down (minus 1), and the Hamiltonian (H) function describes how the interactions between neighboring spins influence the system's total energy.

$$H = -J \sum_{i,j} S_i S_j - h \sum_{i} S_i \tag{1}$$

In Equation (1), S_i and S_j represent neighboring spins, J is the coupling constant, and h denotes the external magnetic field. The Ising model has not only been used to explore the physical properties of magnetic materials but has also been successfully applied in a wide range of areas such as modeling interactions in social networks, analyzing protein-folding processes, and solving complex economic problems [23], [24], [25]. Thus, having evolved into a universal tool for studying social, biological, and physical systems, the Ising model emerges as a valuable method when a detailed examination of spatial relationships is required.

In this regard, the combined use of Voronoi tessellation and the Ising model holds the potential to substantially enhance the general predictive capabilities offered by classical epidemiological models. While Voronoi tessellation provides a more realistic representation of individuals' spatial positions, the Ising model can incorporate interaction strength (e.g., through the J parameter) within this spatial framework, enabling a detailed analysis of local disease spread dynamics. By applying both approaches together, the effects of factors such as proximity and movement patterns among individuals within a community can be evaluated more comprehensively. Although implementing Voronoi and Ising models entails challenges such as high computational requirements and extended simulation times, their ability to deliver detailed spatial resolution offers advantages over classical models particularly for assessing the effectiveness of local intervention strategies and understanding spatial transmission patterns.

Consequently, the integrated use of classical epidemic models, which allow for rapid and analytical forecasts, with Voronoi tessellation and the Ising model, which more realistically account for spatial and interaction dynamics, contributes to a more accurate and in-depth understanding of epidemic processes on both large and local scales. Furthermore, because the Ising model can be extended from regular grids to complex network topologies, it facilitates the study of structures that better mirror real social interaction networks. As a result, it enables more realistic modeling of how "infected" or "healthy" states are updated through interactions among neighboring individuals.

In our study, we present an approach that integrates Voronoi tessellation with an adaptation of the classical Ising model to more realistically model the spread of an infectious disease within a sample population composed of heterogeneously and irregularly distributed individuals. By assigning random initial positions to these individuals, we aim to approximate real-world spatial heterogeneity as closely as possible, thereby overcoming the limitations imposed by the homogeneous mixing assumption. Moreover, the choice of a random distribution is motivated by the fact that real populations often do not exhibit a regular pattern

and instead possess spatially heterogeneous structures. Such a random distribution allows for observation of how interactions occur without relying on a fixed lattice or organized pattern, thus contributing to a more realistic representation of the spatial and interactional factors affecting disease transmission. In this framework, the spatial structure is defined through Voronoi tessellation, while interaction strength among individuals is governed by parameters derived from the Ising model. Within this comprehensive setup, we analyze local-level disease transmission dynamics via Monte Carlo simulations and the Metropolis algorithm, implementing computations in Python and visualizing the outcomes with Matplotlib. We then investigate how the J parameter considered here as a measure of transmissibility affects contact intensity and, consequently, the rate of disease spread. Unlike previous studies that rely on homogeneous mixing or simplified grid assumptions, this approach aims to capture spatial interactions more accurately, thereby offering more reliable insights into the spread of infectious diseases.

2 MATERIAL AND METHOD

In this section, a detailed explanation is provided of the methodology that integrates the Ising model and Voronoi tessellation to model the dynamics of infectious disease spread within a randomly distributed sample population. Additionally, the methodological approach used to analyze how interactions among individuals and their rates of movement affect the transmission of infectious diseases in such a randomly distributed population is summarized, along with the relevant analyses and solutions.

2.1 Formulation of the Model

In this study, the portion of the Ising model's Hamiltonian (H) equation

$$H = -J \sum_{i,j} S_i S_j \tag{2}$$

is employed. In the traditional model, the spin states of each site, originally denoted as -1 and $+1$, are adapted for epidemiological purposes to represent "infected" and "healthy" individuals, respectively. In this context, the parameter S_i corresponds to infected regions, whereas S_j denotes healthy regions. The interaction constant (J) in the model captures the "transmission" or "immunity" interactions arising from neighboring individuals sharing similar or different health statuses. To simplify the system's energy scale and facilitate a broader interpretation of the results, $J = 1$ is used in practice.

In our study, the spatial configuration of the model is generated via a Monte Carlo simulation and the Metropolis algorithm implemented in Python. The initial step of the Monte Carlo simulation involves a randomly selected configuration of the system. During the simulation, a new "trial" state is proposed at each step by altering the infected or healthy status of a single cell, and the corresponding energy change ΔE of the system is computed. According to the Metropolis algorithm, if $\Delta E \leq 0$, the new state is accepted; otherwise, if $\Delta E > 0$, the probability of acceptance is given by

$$p = \min\left(1, \exp(-\beta \Delta E)\right) \tag{3}$$

Here, p is defined based on the principle of detailed balance from the Boltzmann distribution, which ensures that the system converges to equilibrium. In the Python implementation, a random number r in the interval $[0,1]$ is generated for each trial step. If $r < p$ the proposed change is accepted; otherwise, the system reverts to its previous state. Additionally, $\beta = \frac{1}{k_B T}$ where k_B is the Boltzmann constant and T is the system's temperature. In epidemiological terms, temperature (T) can be interpreted as an indicator of protective measures or immunity levels. Higher temperatures correspond to a more random spread of infection (a disordered structure), while at lower temperatures, the presence of control measures leads to a more ordered structure (thereby reducing disease transmission). Within this framework, a specific critical temperature or parameter value may determine whether a small infected group will proliferate throughout the entire population.

In the Monte Carlo method, each cell (originally a spin in the standard model) is selected at random, and a new configuration is tested by flipping its current state "infected" or "healthy." One "Monte Carlo step" (MCS) typically consists of an update cycle in which every cell in the system is tested in sequence. As the simulation proceeds, the statistical behavior of the system is analyzed by monitoring changes in total energy, the average ratio of infected to healthy individuals, or other macroscopic observables. Convergence (or equilibrium) criteria are defined to determine whether the system has reached a stable or quasi-stable state; for instance, if no significant change in macroscopic quantities is observed over a certain number of MCS steps, this indicates that the system has attained equilibrium. Additionally, "warming up" (equilibration) steps are performed at the start of the simulation to eliminate transient effects arising from random initial states, ensuring that the Metropolis algorithm's tendency to "minimize system energy" more realistically reflects the dynamics of disease spread or stabilization. Once equilibrium is reached, the resulting configurations are visualized spatially

using Voronoi diagrams. At this stage, each “core” center (either an infected or a healthy individual) serves as the basis for partitioning the space into regions closest to that center; regions corresponding to infected centers are shown in blue, whereas those corresponding to healthy centers are shown in red. This approach makes it possible to clearly examine the spatial distribution of the infection, along with any clustering or spreading tendencies, and to demonstrate how local interactions shape the macro-scale behavior of the model.

Figure 1 presents the first Voronoi diagram generated by the Monte Carlo simulation and Metropolis algorithm based on Equation (2), illustrating the random distribution of infected and healthy regions as well as their mutual interactions:

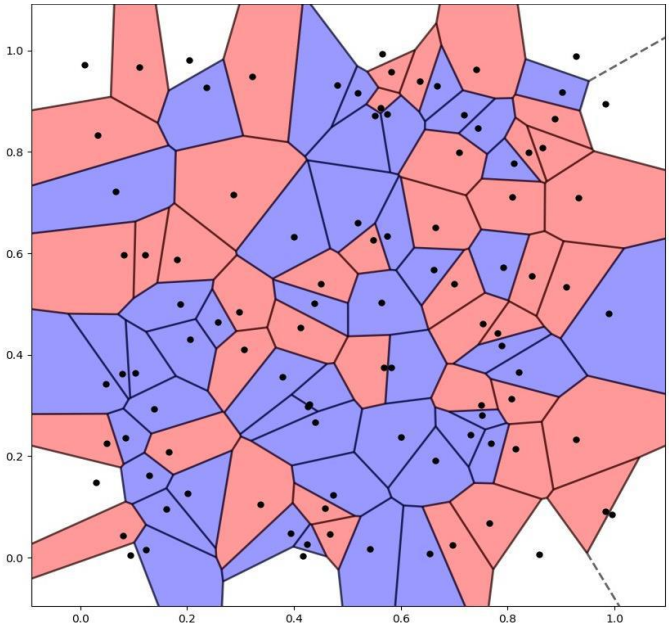

Figure 1. Initial state of the Voronoi diagram.

Figure 2 presents the Voronoi diagram obtained after the first iteration, illustrating the redistribution of infected and healthy regions and the new spatial arrangement that emerges compared to the initial state:

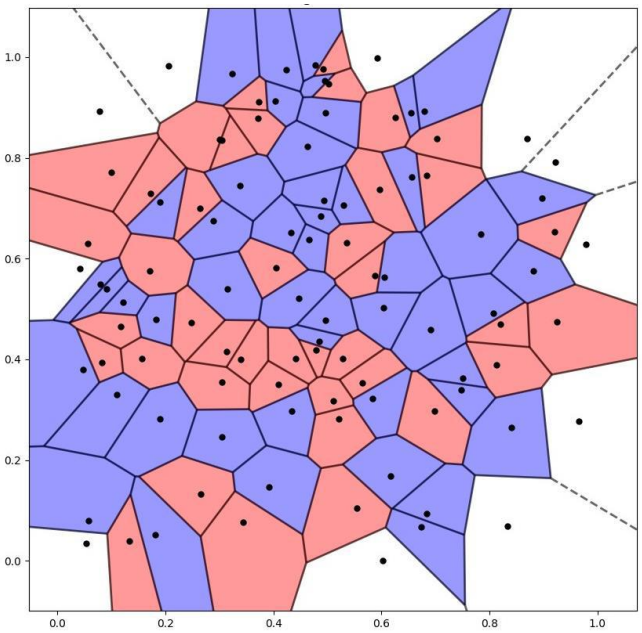

Figure 2. Iteration 1 state of the Voronoi diagram.

Figure 3 presents the diagram obtained at the end of the second iteration, where the final state of the model's spatial dynamics and the ultimate interactions between infected and healthy regions can be observed:

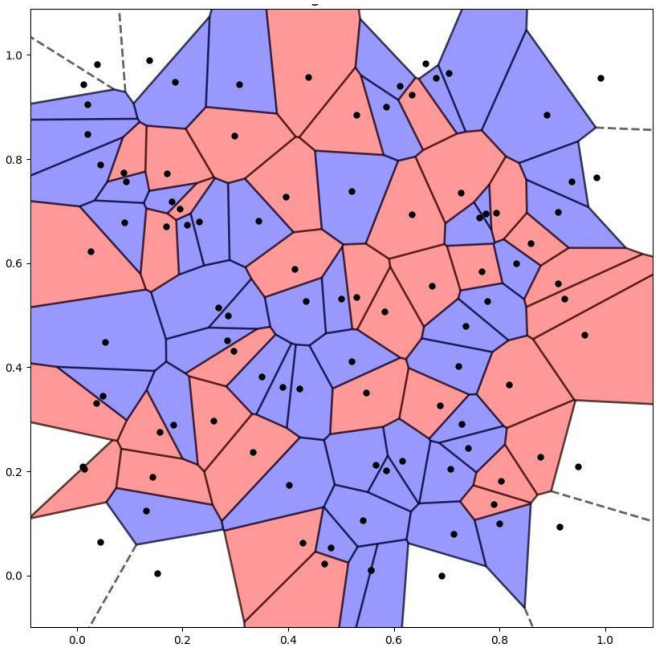

Figure 3. Iteration 2 state of the Voronoi diagram.

2.2 Determination of the Number of Blue and Red Regions

Table 1 presents a dataset showing the relationship between the number of blue and red regions and the system's energy value (H). In the initial state, the energy value was determined to be 16, with the number of blue regions observed as 48 and red regions as 42. In Iteration 1, the energy value dropped to -4, while the number of blue regions remained constant at 48, and the number of red regions decreased to 41. In Iteration 2, the energy value increased to 24, with the number of blue regions rising to 51, while the number of red regions decreased to 37. These data clearly illustrate how numerical changes in the regions throughout the iterations are related to energy.

Table 1. Number of blue and red regions.

	Energy (H)	**Number of Blue Regions**	**Number of Red Regions**
Initial State	16	48	42
Iteration 1	-4	48	41
Iteration 2	24	51	37

2.3 Histogram Analysis of the Polygon Areas of Voronoi Cells

The Histogram analyses were conducted to examine the distribution of polygonal areas of the Voronoi cells obtained at each iteration for both infected (blue) and healthy (red) regions. In these analyses, the horizontal axis (x-axis) represents a specific range of polygon areas (i.e., the total number of cells within that range), while the vertical axis (y-axis) shows the number of polygons that fall within that range. Presented separately for the initial state, the first iteration, and the second iteration, these histograms enable visualization of the dynamics of disease spread or the preservation of healthy tissue; an increase in column height indicates a higher frequency of polygons within that area range. Consequently, both the spatial development of infected regions and the preservation level of healthy regions can be quantitatively and comparatively assessed over time.

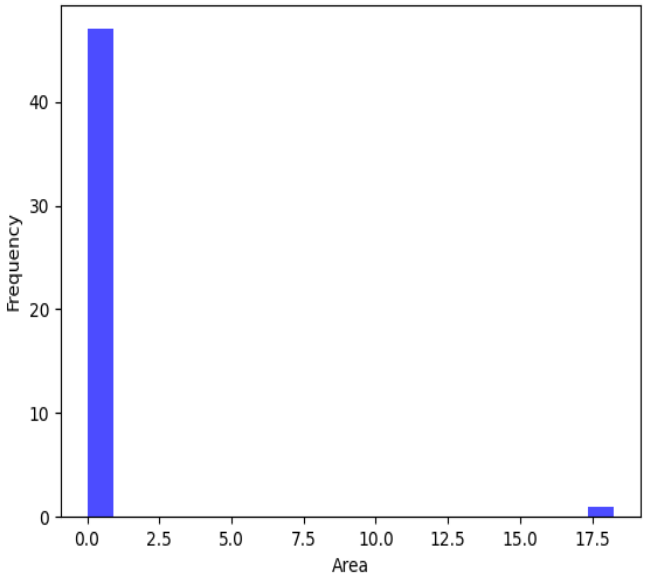

Figure 4. Histogram of blue regions in the Initial state.

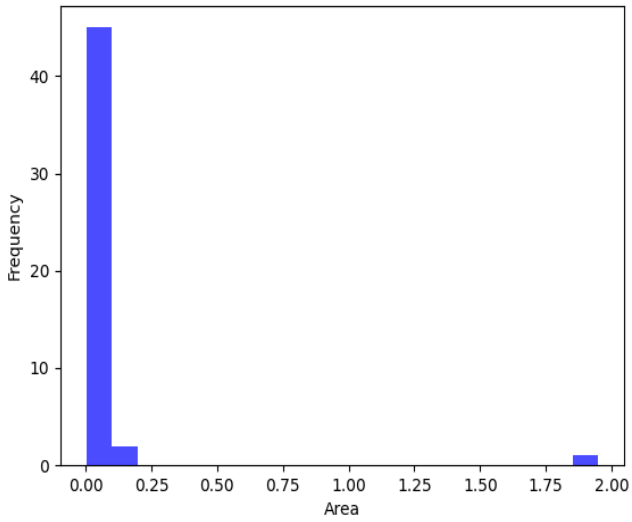

Figure 5. Histogram of blue regions in Iteration 1.

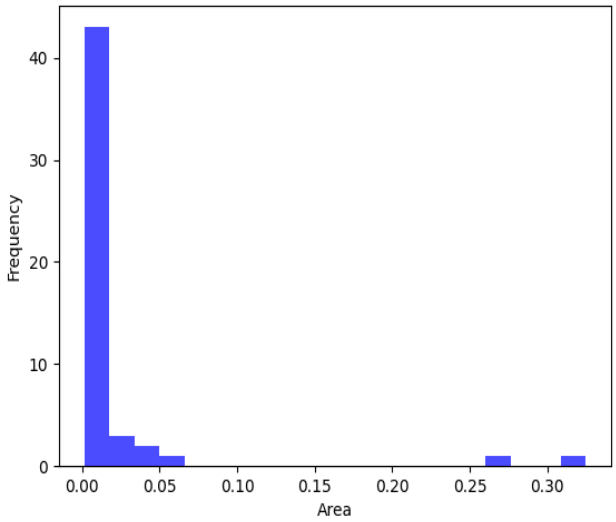

Figure 6. Histogram of blue regions in Iteration 2.

In Figure 4, which depicts the initial state, the histogram shows that most infected regions cluster within small areas, while large-area infected regions are either very few or virtually absent. From an epidemiological standpoint, this distribution suggests an early or partial spread of the infection, with no substantial clustering yet. In Figure 5, presenting the histogram after the first iteration, small infected areas still predominate; however, there is also an observable increase in the frequency of larger infected areas. This trend indicates that some infected regions are merging or expanding to form larger clusters, thereby implying that the infection has begun to spread within the host tissue. Finally, in the second iteration histogram shown in Figure 6, a slight decrease or stabilization is noted in the number of small infected areas, whereas medium and large infected areas exhibit a moderate increase. This finding suggests that the infection continues to spread and consolidate over time, with the pathogen propagating further and the infected tissues merging into larger contiguous areas.

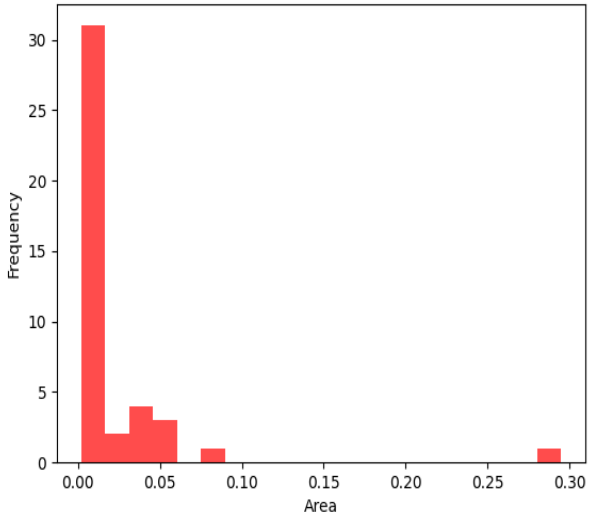

Figure 7. Histogram of red regions in the Initial state.

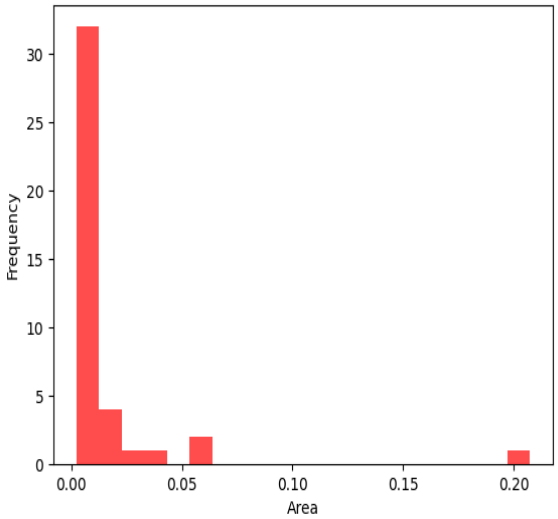

Figure 8. Histogram of red regions in Iteration 1.

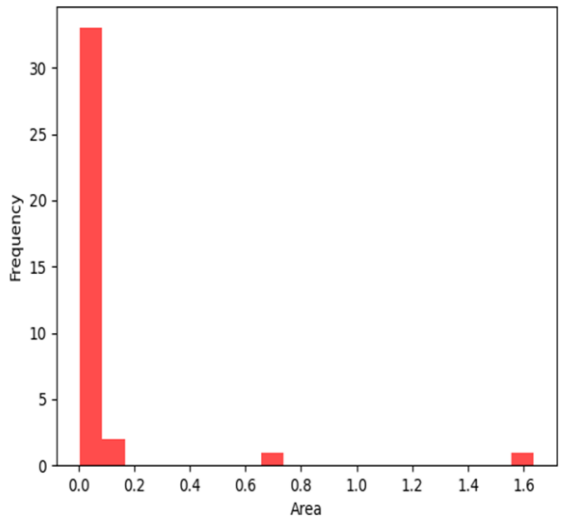

Figure 9. Histogram of red regions in Iteration 2.

In Figure 7, which depicts the initial state, the histogram indicates that healthy regions are primarily concentrated in small- to medium-sized areas and that a substantial portion of the tissue remains unaffected by infection. From an epidemiological standpoint, this early or partial phase suggests that a significant segment of the host tissue has not yet been impacted, and numerous small- or medium-scale healthy foci still exist. After the first iteration, as shown in Figure 8, a slight decrease or redistribution can be observed in the frequency of small healthy regions, yet large healthy areas remain prominent. This observation implies that although the infection has begun to spread, extensive portions of the host tissue continue to harbor healthy cells, and regions resistant or not yet exposed to the infection persist. Finally, the second iteration, presented in Figure 9, reveals a notable decrease or shift in the number of small- to medium-sized healthy regions, indicating that as the infection advances, healthy tissues recede to some extent and certain areas transition to infected regions. At this stage, the diminished or contracted presence of large-scale healthy areas reflects the ongoing interaction between pathogen spread and host defense mechanisms, suggesting that the disease has progressed further and is challenging the host's capacity to maintain healthy tissue.

2.4 Iteration for Different J Values

At this stage, the interaction constant, initially set to $J = 1$, was varied to $J = 3$ and $J = -3$, and analyses were performed for each of these values. In addition, the steps for determining the number of regions and visualizing cell areas are described in Section 2.2. and 2.3., were repeated for each new J value. This approach aims to demonstrate the model's behavior under

different interaction constants and to assess how these parameter changes influence the system's dynamics.

For $J = 3$

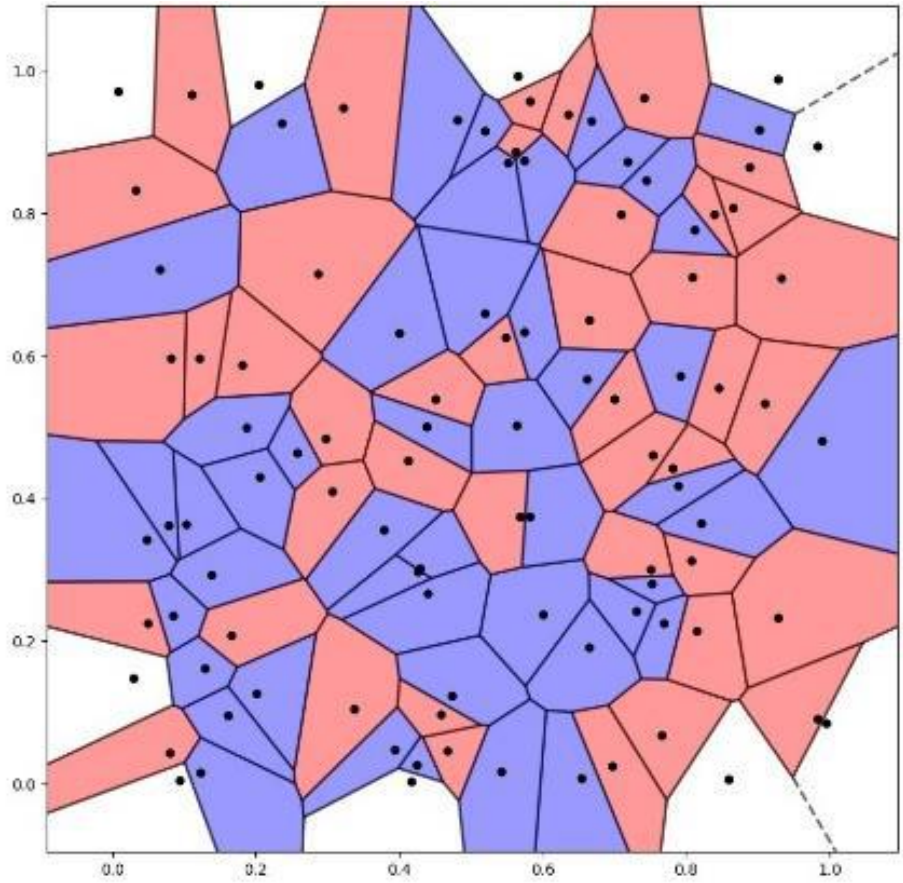

Figure 10. Voronoi diagram of the Initial state for $J = 3$.

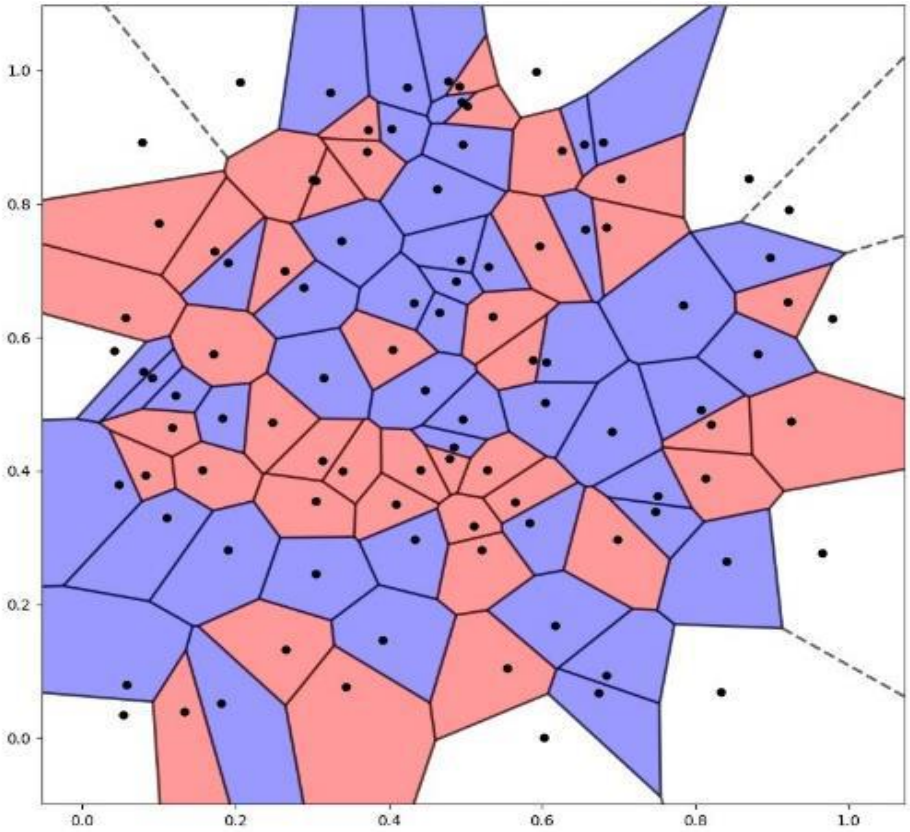

Figure 11. Voronoi diagram of Iteration 1 for $J = 3$.

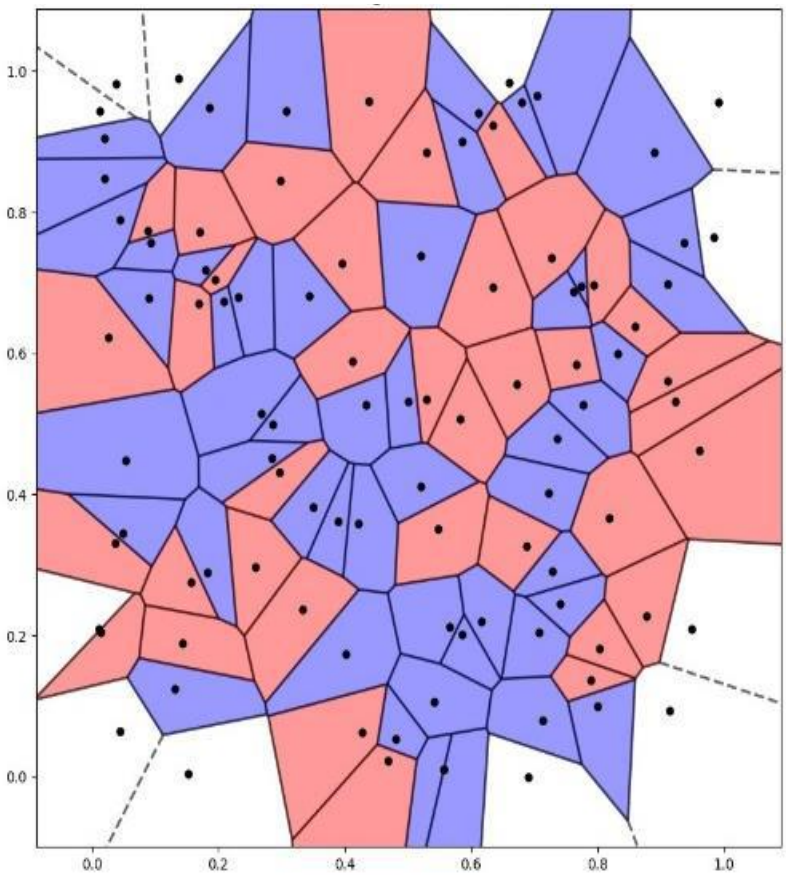

Figure 12. Voronoi diagram of Iteration 2 for $J = 3$.

Table 2. Number of blue and red regions $J = 3$.

	Energy (H)	Number of Blue Regions	Number of Red Regions
Initial Status	48	48	42
Iteration 1	-12	48	41
Iteration 2	72	51	37

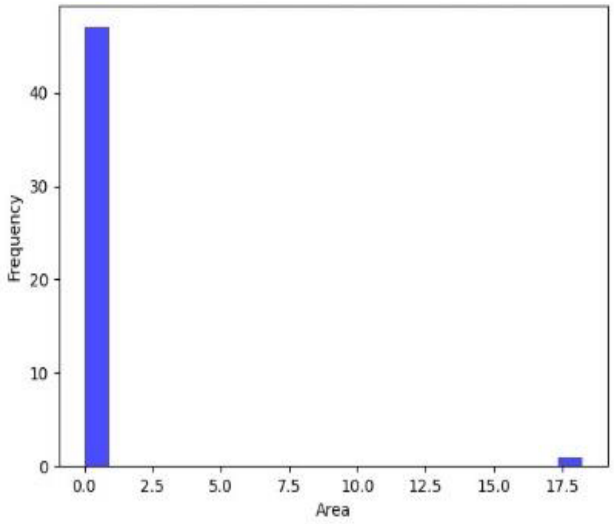

Figure 13. Histogram of blue regions in the Initial state for $J = 3$.

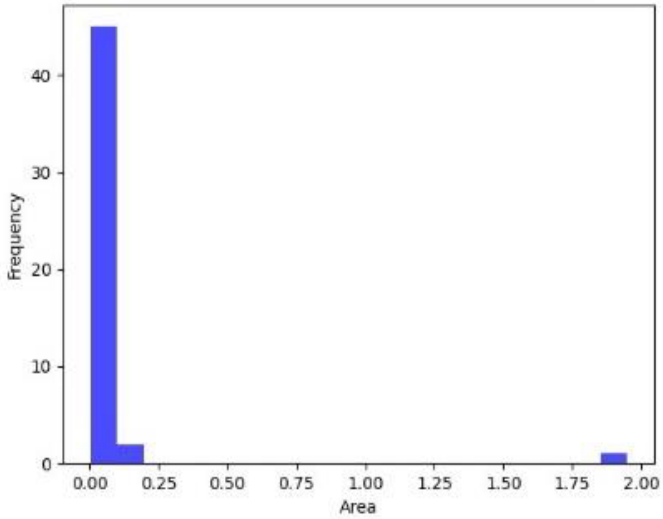

Figure 14. Histogram of blue regions in Iteration 1 for $J = 3$.

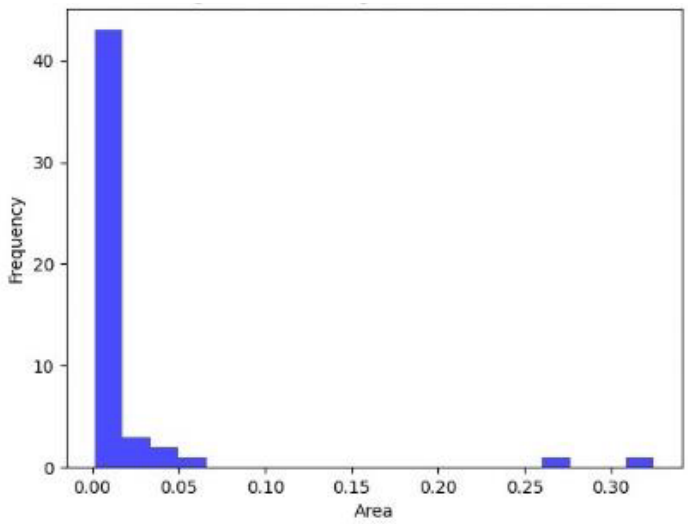

Figure 15. Histogram of blue regions in Iteration 2 for $J = 3$.

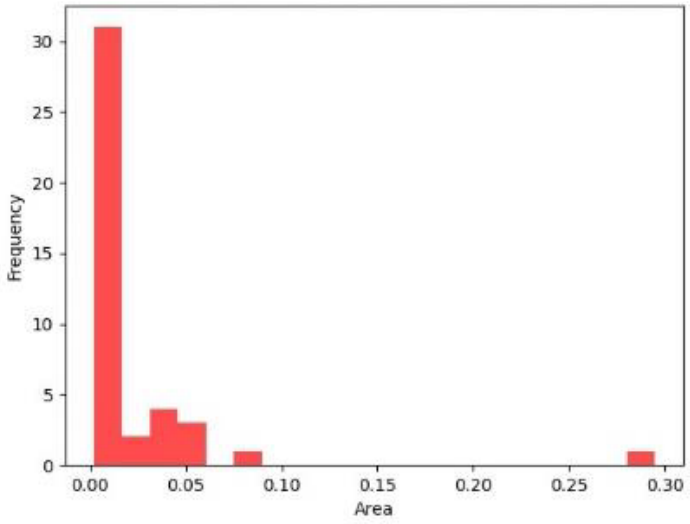

Figure 16. Histogram of red regions in the Initial state for $J = 3$.

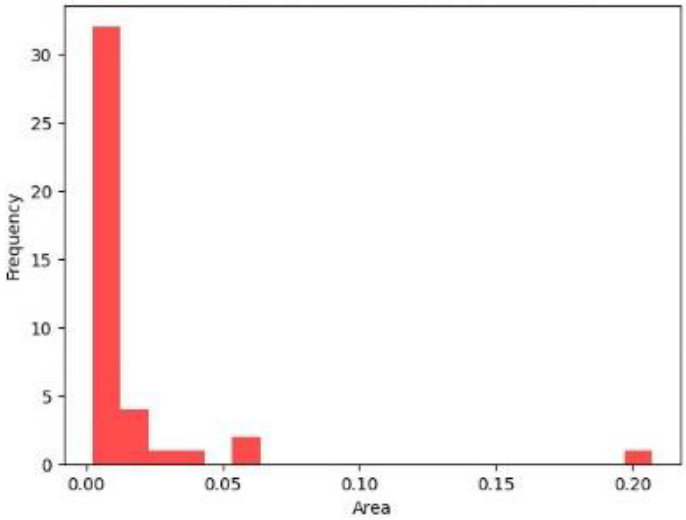

Figure 17. Histogram of red regions in Iteration 1 for $J = 3$.

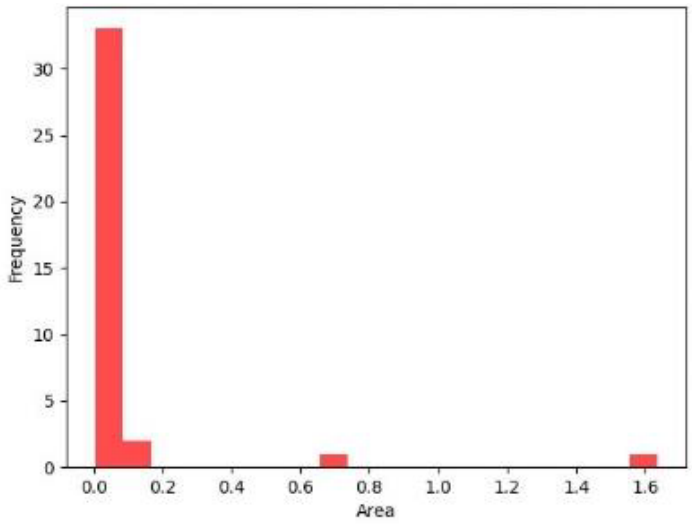

Figure 18. Histogram of red regions in Iteration 2 for $J = 3$.

The Voronoi diagrams (Figures 10, 11, and 12), along with Table 2 and the histograms (Figures 13–18) obtained from the system with $J = 3$, offer both numerical and visual perspectives on infection spread and the preservation of healthy tissue. The results in Table 2, which detail the total energy (H) calculated at each iteration as well as changes in the number of blue (infected) and red (healthy) regions, reflect the system's statistical equilibrium and the intensity of interactions among tissues. Notably, the increase in the number of infected regions by the end of the second iteration suggests that, under $J = 3$, the infection's spread becomes more pronounced. The Voronoi diagrams provide a comparative view of the spatial distribution of infected (blue) and healthy (red) areas over time. While the initial state appears relatively homogeneous, subsequent iterations show infected areas expanding and merging, while healthy areas shrink into isolated "islands." This spatial transformation indicates that a $J = 3$ value supports stronger intercellular interactions and clustering of the infectious agent. Meanwhile, the histograms present the frequency distribution of blue and red regions by area size for each iteration, thereby numerically confirming the expansion of infected tissue and the contraction of healthy tissue. Over time, smaller infected regions merge to form medium and large clusters, whereas healthy regions become confined to increasingly smaller areas. These findings imply that infection propagation intensifies at $J = 3$, while the capacity of healthy tissue to resist infection becomes more constrained.

For $J = -3$

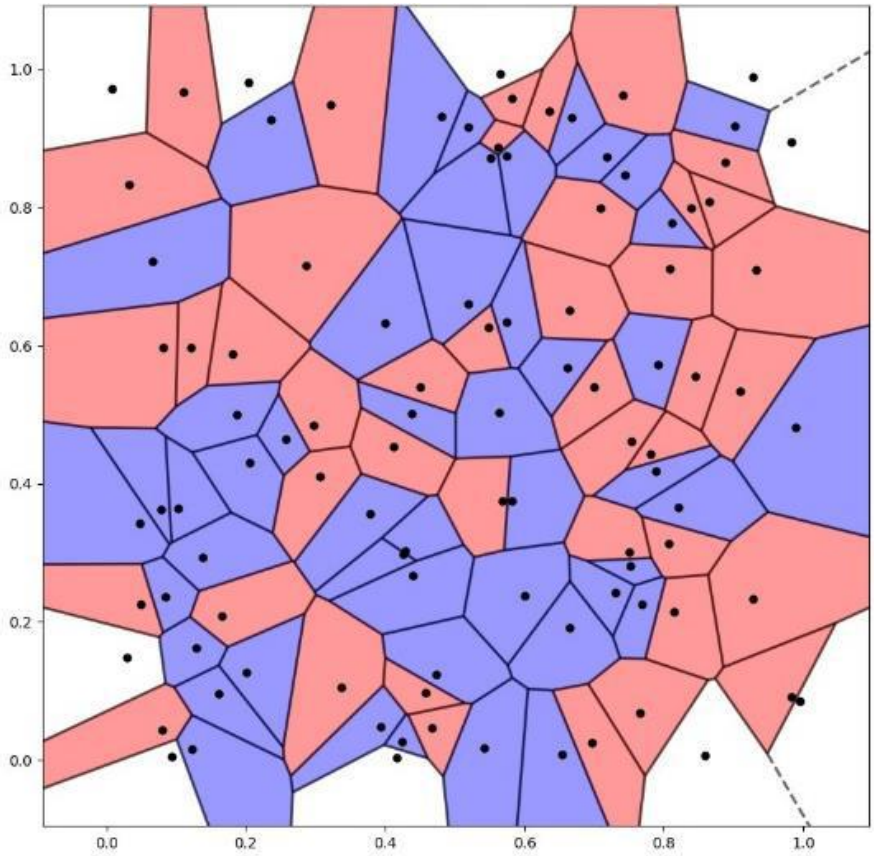

Figure 19. Voronoi diagram of the Initial state for $J = -3$.

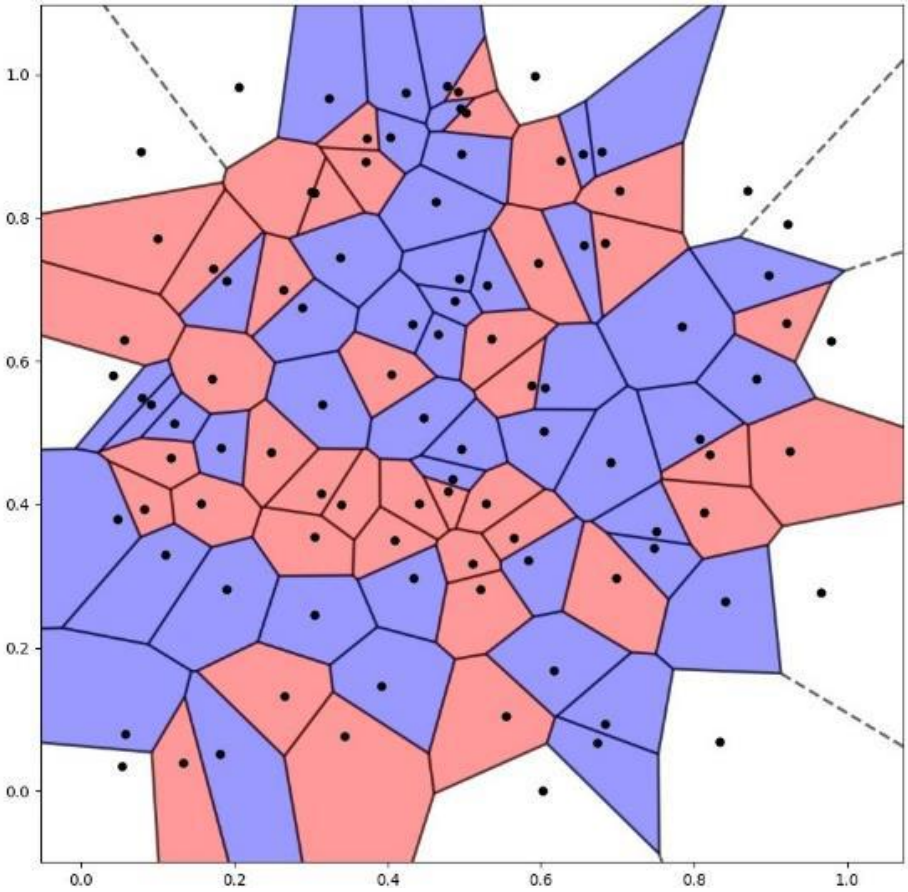

Figure 20. Voronoi diagram of Iteration 1 for $J = -3$.

Table 3. Number of blue and red regions $J = -3$.

	Energy (H)	Number of Blue Regions	Number of Red Regions
Initial Status	-48	48	42
Iteration 1	12	48	41

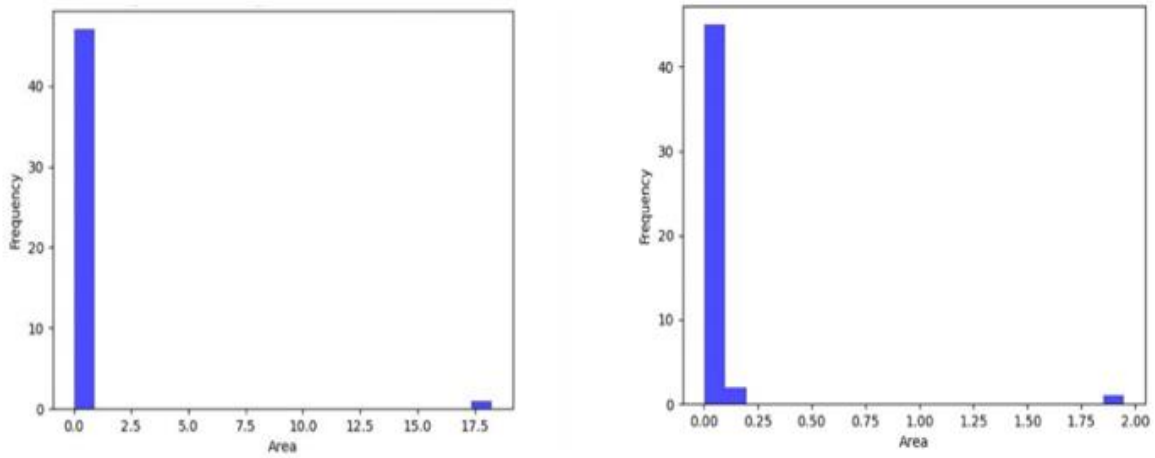

Figure 21. Histogram of blue regions for $J = -3$

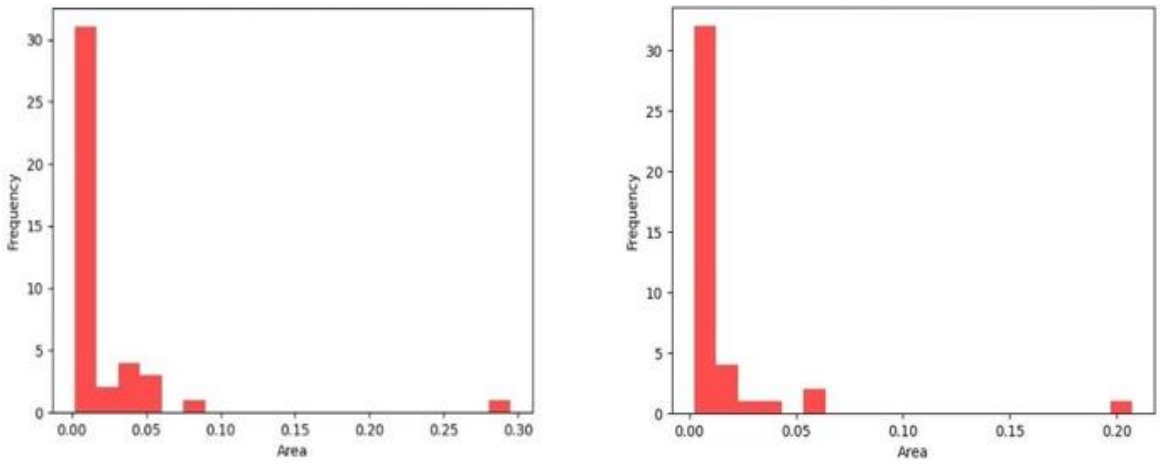

Figure 22. Histogram of red regions for $J = -3$

The Voronoi diagrams (Figure 19-20), Table 3, and histograms (Figure 21-22) obtained under $J = -3$ illustrate changes in the model dynamics for infected (blue) and healthy (red) regions. The energy (H) and region count values in Table 3 suggest that, under this negative coupling constant, the spread of infection is stabilized within certain limits, resulting in no marked shifts in the number of infected or healthy regions. The Voronoi diagrams support this observation from a spatial standpoint: compared to the initial state, only limited interaction is

observed, and there is no evident trend toward significant infection spread. Meanwhile, the histograms indicate that both infected and healthy regions predominantly remain in small and medium sized areas, quantitatively confirming the lack of tendencies such as the merging of infected regions into larger clusters or a rapid contraction of healthy areas. Only a single iteration is presented for $J = -3$ because, under this negative coupling condition, the system reaches a relatively stable distribution at an early stage.

3 RESULTS AND DISCUSSION

In this section, the effects of different values of J on the number of blue (infected) and red (healthy) regions are evaluated in detail from the initial stage through each iteration. The findings indicate that J plays a decisive role in disease spread dynamics and that varying transmission coefficients significantly influence the distribution of healthy and infected regions. Positive J ($J = 1$ or $J = 3$) replicates ferromagnetic interactions, promoting alignment among neighboring cells in similar states, which in turn leads to the merging and expansion of infected regions.

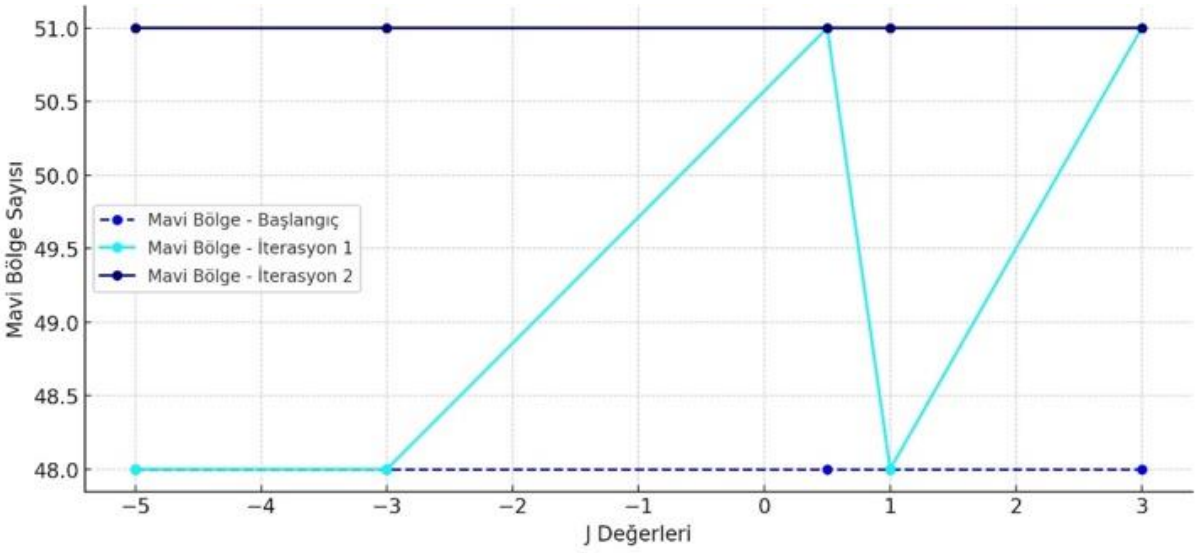

Figure 23. Change in the number of blue regions according to J values (Initial state and Iterations)

This outcome may reflect conditions such as high contact rates, insufficient vaccination, or inadequate preventive measures within the population. By contrast, negative J ($J = -3$) represents antiferromagnetic interactions, facilitating the coexistence of neighboring cells in different states; under such circumstances, the presence of interventions like vaccination and social distancing can limit disease transmission and enable early stabilization.

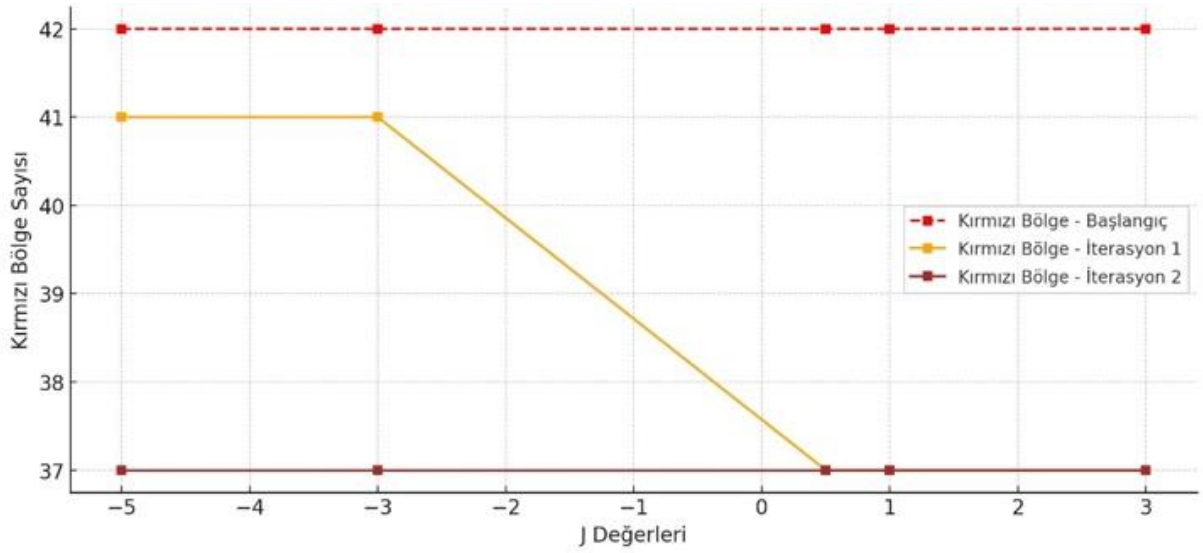

Figure 24. Change in the number of red regions according to J values (Initial state and Iterations).

The numerical data confirm that infection progresses more rapidly under positive J values, whereas it is suppressed under negative J values. Consequently, this model provides a comprehensive framework that can aid in optimizing disease control strategies when spatial distribution and inter-individual interactions are considered in conjunction with epidemiological measures (e.g., vaccination and social distancing).

4 CONCLUSION AND SUGGESTIONS

This study introduces a novel approach that integrates Voronoi tessellation with the Ising model to investigate the spatial interactions and mobility among individuals in a randomly distributed sample population. Simulations performed under different transmission coefficients (***J*** values) clearly demonstrate that the dynamics of disease spread are strongly influenced by both the magnitude and the sign of ***J***. Notably, positive ***J*** values, which can be associated with high contact rates, low vaccination levels, and inadequate preventive measures, lead to faster and more widespread disease transmission. In contrast, negative ***J*** values simulating effective vaccination, social distancing, and robust interventions suppress transmission and help preserve healthy regions.

By offering a more realistic representation of spatial heterogeneity and local interactions, this model addresses a critical gap in conventional epidemiological approaches that rely on homogeneous mixing assumptions. The findings indicate that altering ***J*** values through increased vaccination, the implementation of social distancing, or the adoption of other

protective measures can significantly affect the trajectory of an outbreak. Consequently, this framework enables a comprehensive assessment of both local infection cluster dynamics and the broader impacts of interventions, thus facilitating the development of more targeted public health strategies.

Acknowledgment

This study is derived from the Master's thesis of the first authors, titled "Dynamical Modeling of an Infectious Disease Using an Ising Model Constructed on Voronoi Tessellation", and was supported by Fırat University Scientific Research Projects (BAP) Coordination Unit (Project No. FF.24.21).

Conflict of Interest Statement

There is no conflict of interest between the authors.

Statement of Research and Publication Ethics

The study is complied with research and publication ethics.

Artificial Intelligence (AI) Contribution Statement

In this study, artificial intelligence (AI) tools were used solely for purpose of improving the grammatical accuracy and linguistic clarity of the English text. All scientific content, including data analysis, figures, and the manuscript's structural composition, was entirely generated by the authors without any AI assistance.

Contributions of the Authors

The first author played an active role in approximately 70% of the study, including the development of the conceptual framework, model design, execution of simulations, data analysis, and manuscript writing. The second author, as the academic advisor of the first author, contributed approximately 30% to the study by providing support in determining the methodological approach, offering academic guidance, and contributing to the scientific evaluation and improvement of the work. Both authors have read and approved the final version of the manuscript.

REFERENCES

[1] R. M. Anderson and R. M. May, *Infectious Diseases of Humans: Dynamics and Control.* Oxford University Press, 1992.

[2] C. J. L. Murray, *Epidemiology of Infectious Disease.* WHO Publications, 2013.

[3] S. Hsiang, et al., "The Effect of Large-Scale Anti-Contagion Policies on the COVID-19 Pandemic", Nature, 2020, pp. 262-267.

[4] D. Herlihy, *The Black Death and the Transformation of the West.* Harvard University Press.

[5] N. P. Jonhson, J. Mueller, "Updating the Accounts: Global Mortality of the 1918-1920 'Spanish' Influenza Pandemic", Bulletin of the History of Medicine, 2002, pp. 105-115.

[6] P. Piot, et al., "HIV/AIDS in Africa: Global Responses and Challenges", Science, 2001, pp. 2149-2150.

[7] S. M. Kissler, et al., "Projecting the Transmission Dynamics of SARS-CoV-2 through the Postpandemic Period", Science, 2020, pp. 860-868.

[8] F. Brauer, et al., *Mathematical Models in Epidemiology.* Springer, 2012.

[9] K. Dietz, J. A. P. Heesterbeek, "Daniel Bernoulli's Epidemiological Model Revisited", Mathematical Biosciences, 2002, pp. 1-21.

[10] W. O. Kermack, and A. G. McKendrick, "A Contribution to the Mathematical Theory of Epidemics", Proceeding of the Royal Society A, 1927, pp. 700-721.

[11] M. Keeling, and P. Rohani, *Modeling Infectious Disease in Humans and Animals*. Princeton University Press, 2008.

[12] Z. Fengi, "Applications of SEIR Models in Epidemiology", Advances in Epidemiological Modeling, 2007, pp. 97-112.

[13] R. Singh, S. Ali, M. Jain, A. A. Raina, "Mathematical Model for Malaria with Mosquito-Dependent Coefficient for Human Population with Exposed Class", Journal of the National Science Foundation of Sri Lanka, 2019, pp. 185-198.

[14] A. A. Raina, S. Ali, P. Kalra, U. M. Modibbo, "A Mathematical Model of Logistic Human Population Growth and Vector Population for Dengue Transmission Dynamics", Journal of the Egyptian Society, 2024, pp. 23-55.

[15] O. Diekmann, et al., *Mathematical Tools for Understanding Infectious Disease Dynamics.* Princeton University Press, 2013.

[16] V. Colizza, et al., "Modeling the Worldwide Spread of Pandemic Influenza: Baseline Case and Containment Interventions", PLoS Medicine, 2007.

[17] A. Okabe, B. Boots, K. Sugihara, S. N. Chiu, *Spatial Tessellations: Concepts and Applications of Voronoi Diagrams.* John Wiley & Sons, 2009.

[18] M. Menezes, et al., "Using Voronoi Diagrams for Spatial Dynamics in Disease Modeling", Journal of Spatial Simulation, 2010.

[19] B. Boots, et al., "Voronoi Tessellation and Its Applications in Spatial Modeling", Geographical Analysis, 2006.

[20] T. Suzuki, and N. Egami, "Applications of Voronoi Diagrams in Neuron Distribution Analysis", Computational Biology, 2006.

[21] E. Ising, "Beitrag zur Theorie des Ferromagnetismus", Zeitschrift für Physik, 1925, pp. 253-258.

[22] S. G. Brush, "History of the Lenz-Ising Model", Review of Modern Physics, 1967, pp. 883-893.

[23] R. J. Glauber, "Time-dependent Statistics of the Ising Model", 1963, pp. 294-307.

[24] L. Onsager, "Crystal Statistics. I. A Two-dimensional Model with an Order-Disorder Transition", Physical Review Journals Archive, 1944, pp. 117-149.

[25] C. Castellano, S. Fortunato, and V. Loreto, "Statistical Physics of Social Dynamics", Review of Modern Physics, 2009, pp. 591-646.